




Article

Development of a Gold Nanoparticle-Based Amplification-Free Nanobiosensor for Rapid DNA Detection Supported by Machine Learning

Yunus Aslan ¹ , Yeşim Taşkın Korucu ², Brad Day ³  and Remziye Yılmaz ^{2,*} 

¹ Department of Electrical and Electronics Engineering, Middle East Technical University, 06800 Ankara, Turkey; aslany@metu.edu.tr

² FoodOmics Laboratory, Department of Food Engineering, Hacettepe University, 06800 Ankara, Turkey; yesim.0197@gmail.com

³ East Tennessee Health Innovation Alliance, Associate Vice Chancellor & Executive Director, University of Tennessee, Knoxville, TN 37996, USA; bradday@utk.edu

* Correspondence: remziye@hacettepe.edu.tr

Abstract

The global expansion of genetically modified (GM) crop cultivation has increased the demand for analytical platforms that can provide rapid, reliable, and cost-effective detection of GM-derived ingredients to support traceability, regulatory compliance, and accurate labeling. Conventional molecular assays such as polymerase chain reaction (PCR) and isothermal amplification are highly sensitive and specific but depend on sophisticated instrumentation and trained personnel, limiting their applicability in field settings. Here, we present a label-free and amplification-free nanobiosensor based on citrate-capped gold nanoparticles (AuNPs) for the direct colorimetric detection of the Cry1Ac gene associated with the MON87701 soybean event, without the use of polymerase chain reaction (PCR) or any enzymatic nucleic acid amplification step. The assay relies on the localized surface plasmon resonance (LSPR) of AuNPs, which induces a red-to-purple color transition upon hybridization between complementary DNA strands. Critical reaction parameters, including NaCl concentration, AuNP size, and ionic strength, were optimized to enable selective and reproducible aggregation. Integration with a Support Vector Machine (SVM) algorithm enabled automated spectral classification and semi-quantitative discrimination of GM content levels. The optimized AuNP–SVM system achieved high sensitivity (limit of detection $\approx 2.5 \text{ ng } \mu\text{L}^{-1}$, depending on nanoparticle batch), strong specificity toward Cry1Ac-positive sequences, and reproducible classification accuracies exceeding 90%. By eliminating enzymatic amplification steps, the proposed platform significantly reduces assay time, operational complexity, and instrumentation requirements, making it suitable for rapid on-site GMO screening.

Keywords: gold nanoparticles; colorimetric biosensor; GMO detection; Cry1Ac; amplification-free DNA detection; machine learning



Received: 26 January 2026

Revised: 15 February 2026

Accepted: 19 February 2026

Published: 20 February 2026

Copyright: © 2026 by the authors.

Licensee MDPI, Basel, Switzerland.

This article is an open access article distributed under the terms and conditions of the [Creative Commons Attribution \(CC BY\) license](https://creativecommons.org/licenses/by/4.0/).

1. Introduction

Genetically modified (GM) crops have significantly advanced modern agriculture by enabling precise modification of plant genomes to introduce advantageous traits unattainable through conventional breeding [1]. Through the application of molecular biotechnology, crop genomes can be selectively engineered to enhance agronomic performance,

environmental adaptability, and nutritional quality [2]. As a result, GM crops have contributed to improved resistance to pests and pathogens, increased tolerance to abiotic stress conditions such as drought and salinity, and optimized nutrient composition, providing substantial agronomic and economic benefits worldwide [3,4].

Since the commercialization of the first genetically modified crop, the FlavrSavr tomato, in 1994, the global cultivation of biotechnology-derived crops has expanded rapidly [5]. By 2024, approximately 206.3 million hectares of farmland worldwide were devoted to GM crops, with regulatory approval granted in more than 30 countries [6]. In response to this widespread adoption, science-based regulatory frameworks have been established to ensure that GM crops are assessed, authorized, and monitored in a transparent and evidence-driven manner. In the European Union, the European Food Safety Authority (EFSA) conducts comprehensive, case-by-case risk assessments of genetically modified plants prior to authorization, focusing on molecular characterization, food and feed safety, and potential environmental effects [7].

In addition to pre-market evaluation, EFSA requires post-market environmental monitoring (PMEM) to identify any unanticipated or long-term effects that may arise following large-scale cultivation and commercialization of approved GM events [7]. This precautionary yet evidence-based monitoring strategy aims to support traceability, regulatory compliance, and ongoing oversight within complex agri-food systems, rather than implying inherent risk associated with authorized GM crops. Accordingly, mandatory labeling and monitoring requirements have been implemented to facilitate effective market surveillance and international trade. For example, the European Union (EU) requires labeling when GM content exceeds 0.9% per ingredient [8], underscoring the need for reliable analytical methods capable of accurately detecting GM components throughout the food supply chain.

A wide range of analytical strategies has been developed for the detection of GM crops, including molecular, immunological, and biosensing-based approaches. Molecular techniques such as polymerase chain reaction (PCR) [9], real-time PCR [10,11], digital PCR [12], and isothermal amplification methods [13,14] are widely employed due to their high sensitivity and specificity. Immunological assays, including enzyme-linked immuno-sorbent assays (ELISA) [15] and lateral flow test strips [16,17], provide rapid and user-friendly alternatives suitable for field applications. In parallel, emerging biosensor platforms have attracted increasing attention for their potential to deliver rapid, on-site, and cost-effective detection [18,19], with recent developments in label-free nanobioelectronic biosensors [20].

Although molecular-based methods provide excellent analytical performance, they typically require sophisticated instrumentation, skilled personnel, and multi-step laboratory workflows. These requirements limit their suitability for routine large-scale screening and decentralized monitoring applications. Consequently, there is a growing demand for rapid, user-friendly, and cost-effective analytical alternatives capable of delivering reliable results without reliance on complex laboratory infrastructure.

In this context, DNA-based biosensors have emerged as a promising class of analytical tools for the detection of GM-associated genes. Among these, citrate-stabilized gold nano-particle (AuNP)-based colorimetric assays are particularly attractive due to their excellent aqueous dispersibility and characteristic localized surface plasmon resonance (LSPR) absorption near 520 nm [21,22]. These optical properties enable direct, label-free, and visually interpretable detection of target DNA sequences through salt-induced nanoparticle aggregation. Several amplification-free AuNP-based colorimetric strategies have been reported for direct detection of unamplified genomic DNA, demonstrating the feasibility of PCR-independent diagnostic platforms for rapid and portable nucleic-acid analysis [23].

The analytical performance of AuNP-based colorimetric assays is strongly influenced by nanoparticle physicochemical properties, including size, surface chemistry, and batch-to-batch variability. In citrate-stabilized systems, aggregation behavior depends critically on ionic strength and nanoparticle size, with smaller AuNPs typically requiring lower salt concentrations to induce aggregation due to differences in electrostatic stabilization and surface curvature effects. This size-dependent aggregation behavior has been previously reported and represents a key parameter that must be carefully optimized to ensure reproducible sensing performance [24].

In this work, a gold nanoparticle-based biosensing platform integrated with machine learning was developed, as schematically illustrated in Figure 1, for the detection of the Cry1Ac gene specific to the MON87701 genetically modified soybean event. Genomic DNA was extracted and analyzed using a salt-induced colorimetric assay in which AuNP aggregation produced a quantifiable spectral shift [25,26]. To address variability arising from nanoparticle size, concentration, and batch-to-batch physicochemical differences, the bio-sensor was integrated with machine learning using a support vector machine (SVM) classifier [27]. While conventional ratiometric analysis (OD620/OD520) enables qualitative discrimination, it may be insufficient to ensure robust and reproducible classification across multiple nanoparticle batches. The SVM-based model was therefore employed to capture nonlinear relationships within the spectral data, improve tolerance to optical variability, and enable reliable semi-quantitative discrimination of GMO content levels, rather than absolute regulatory quantification.

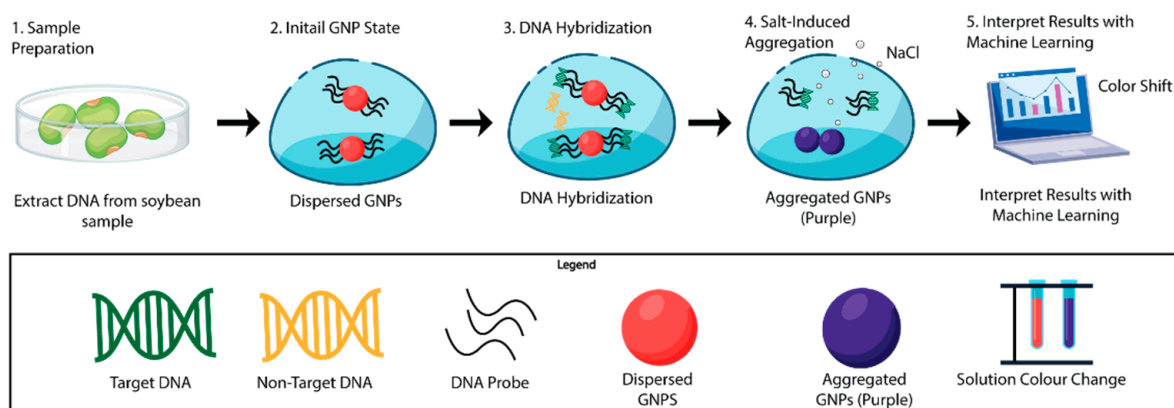


Figure 1. Schematic illustration of the AuNP-based biosensing platform integrated with machine learning for detection of the Cry1Ac gene specific to the MON87701 GM soybean event. The workflow includes (1) genomic DNA extraction from soybean samples, (2) dispersion of citrate-stabilized AuNPs functionalized with complementary DNA probes, (3) probe–target hybridization in the presence of Cry1Ac sequences, (4) NaCl-induced aggregation of AuNPs in the absence of complementary targets resulting in a red-to-purple color shift and corresponding spectral change, and (5) interpretation of colorimetric and spectral responses using SVM classifier for discrimination of GM and non-GM samples.

Although AuNP-based colorimetric DNA assays for GMO detection have been previously reported, based on hybridization-triggered salt-induced aggregation, the present study introduces several key advancements. These include direct amplification-free detection of an event-specific GMO marker using genomic DNA, systematic optimization and evaluation across multiple AuNP batches, and the integration of machine learning as a data-driven strategy rather than a post hoc visualization tool. This combined nanoplasmonic-machine learning framework distinguishes the present work from existing AuNP-based colorimetric GMO assays and provides a robust foundation for intelligent, field-deployable GMO screening platforms.

2. Materials and Methods

2.1. Chemicals and CRMs

Certified reference materials (CRMs) were obtained for genomic DNA-based detection using the AuNP biosensing platform. Two soybean reference materials were purchased from the American Oil Chemists' Society (AOCS): non-modified soybean (AOCS 0906-A2, <0.08% *w/w* GM) and MON87701 soybean (AOCS 0809-A2, $\geq 98.4\%$ *w/w* GM). A Roundup Ready® (RR) soybean blank material (ERM-BF410ak, <0.07% *w/w* GM) was obtained from the Institute for Reference Materials and Measurements (IRMM, Geel, Belgium), and MON15985 cotton (AOCS 0804-D2, $\geq 99.6\%$ *w/w* GM) was also supplied by AOCS. According to the certificates of analysis, AOCS 0809-A2 contained $\geq 98.4\%$ (*w/w*) MON87701 soybean (measurement uncertainty $\pm 0.8\%$ *w/w*, event-specific real-time PCR) with 99.2% purity at a 95% confidence level. The non-modified soybean material (AOCS 0906-A2) was verified to be free of MON87701, MON89788, MON87705, MON87708, MON87751, and MON87769 events (<0.08% *w/w*). ERM-BF410ak was certified as GM-free (<0.07% *w/w* GTS 40-3-2 soybean), while AOCS 0804-D2 contained $\geq 99.6\%$ (*w/w*) MON15985 cotton (uncertainty $\pm 0.2\%$ *w/w*, event-specific PCR). All CRMs were stored at +4 °C in the dark until DNA extraction.

2.2. Synthesis and Characterization of Citrate-Capped AuNPs

Hydrogen tetrachloroaurate(III) trihydrate (HAuCl₄·3H₂O) and trisodium citrate dihydrate (C₆H₅Na₃O₇·2H₂O) were purchased from Sigma-Aldrich (St. Louis, MO, USA). All aqueous solutions were prepared using ultrapure water (18.2 MΩ·cm) obtained from a Milli-Q purification system (Millipore, Bedford, MA, USA). Citrate-capped gold nanoparticles (AuNPs) were synthesized following a modified Turkevich–Frens reduction protocol [28,29]. Briefly, an aqueous HAuCl₄ solution (1.0–1.25 mM, 40–100 mL) was heated to a vigorous boil under continuous magnetic stirring, after which a preheated trisodium citrate solution (38.8 mM, 4–10 mL) was rapidly injected. The reaction mixture was maintained at boiling under constant stirring until the solution developed a deep wine-red color within approximately 10–15 min, indicating the formation of colloidal AuNPs. The suspension was then cooled to room temperature under stirring and stored at 4 °C in the dark. Five independent batches (S1, Y5, Y6, Y7, and Y8) were synthesized under varied reagent ratios to assess reproducibility and particle-size uniformity. The precursor concentrations, reagent volumes, and AuNP concentrations are summarized in Table 1. Transmission electron microscopy (TEM) analysis was conducted on an FEI Tecnai F30 microscope (FEI Company, Hillsboro, OR, USA) operated at 300 kV to evaluate nanoparticle morphology and size distribution. For TEM imaging, 3 μL of diluted AuNP suspension was drop-cast onto a carbon-coated copper grid and air-dried at room temperature. Particle diameters were determined by measuring at least 200 nanoparticles per batch from multiple representative micrographs using ImageJ v.1.53 software (NIH, Bethesda, MD, USA) [30].

Table 1. Summary of precursor concentrations, reagent volumes, and resulting AuNP characteristics obtained from UV–Vis measurements at 520 nm.

Batch Number	HAuCl ₄ ·3H ₂ O		C ₆ H ₅ Na ₃ O ₇ ·2H ₂ O		AuNP (nM)
	Concentration (mM)	Volume (mL)	Concentration (mM)	Volume (mL)	
S1	1.11	90	38.80	10	3.75
Y5	1.11	45	38.76	5	4.70
Y6	1.0	50	38.80	5	4.40
Y7	1.25	40	38.80	4	5.96
Y8	1.0	100	38.80	10	4.77

2.3. GMO Detection Assay with the AuNP Nanobiosensor

Genomic DNA was extracted from 100 mg of CRM powder using the GeneMATRIX Food-Extract DNA Purification Kit (EURx, Gdańsk, Poland) following the manufacturer's instructions. All extracts yielded DNA of sufficient concentration and purity for downstream hybridization-based AuNP assays. On average, non-modified soybean CRMs produced $114.6 \text{ ng } \mu\text{L}^{-1}$ DNA ($\text{OD}_{260}/\text{OD}_{280} = 1.78\text{--}1.95$), while GM soybean CRMs yielded $77.1 \text{ ng } \mu\text{L}^{-1}$ DNA ($\text{OD}_{260}/\text{OD}_{280} = 1.72\text{--}2.09$). Roundup Ready[®] soybean and MON15985 GM cotton generated 51.1 and $70.9 \text{ ng } \mu\text{L}^{-1}$, respectively. Commercial soybean samples showed the highest recovery, averaging $595.8 \text{ ng } \mu\text{L}^{-1}$, likely due to finer grinding and improved cell-lysis efficiency. All samples exhibited $\text{OD}_{260}/\text{OD}_{280}$ ratios within the optimal 1.8–2.0 range, confirming high-purity DNA [31].

The purified DNA was eluted in $100 \text{ } \mu\text{L}$ of elution buffer and stored at $-20 \text{ } ^\circ\text{C}$ until use. DNA concentration and purity were determined using a NanoDrop 2000c spectrophotometer (Thermo Fisher Scientific, Waltham, MA, USA) by measuring optical density at 260 nm (OD_{260}) and 280 nm (OD_{280}). The sequences of the target oligonucleotide and complementary probe are listed in Table 2. Colorimetric assays were performed in a total volume of $120 \text{ } \mu\text{L}$, comprising a $20 \text{ } \mu\text{L}$ hybridization mixture containing the complementary probe ($0.08 \text{ } \mu\text{M}$ final concentration) and genomic DNA ($2.5 \text{ ng } \mu\text{L}^{-1}$ final concentration). Thermal processing was conducted using a Nanobiz CubeCycler[®] thermal cycler under the following conditions: denaturation at $95 \text{ } ^\circ\text{C}$ for 10 min , hybridization at $55 \text{ } ^\circ\text{C}$ for 5 min , and cooling to $30 \text{ } ^\circ\text{C}$ for 1 min . Following hybridization, $90 \text{ } \mu\text{L}$ of freshly synthesized AuNP colloid was added and gently vortexed to ensure homogeneity. Aggregation was subsequently induced by adding $10 \text{ } \mu\text{L}$ of $10\times$ phosphate-buffered saline (PBS) containing NaCl to achieve the optimized final ionic strength. Immediately after salt addition, the complete reaction mixture was transferred into a 96-well microplate for optical analysis. UV–visible spectra were recorded between 400 and 700 nm at 10 nm intervals after 1 , 5 , and 10 min using a microplate reader. All spectra were blank-subtracted (PBS and water without AuNPs) and baseline-corrected at 700 nm to remove scattering effects. Fixed volumes and identical well geometry were maintained across all measurements to ensure consistent optical path lengths, and path-length correction was applied where applicable. Each condition was tested in triplicate wells, and ten independent assays ($n = 10$) were performed per AuNP batch. All AuNP-based assays were performed under identical experimental conditions and measurement settings. Finally, wells were photographed under standardized illumination to document colorimetric transitions.

Table 2. Oligonucleotide sequences used for target and complementary probe design in the AuNP-based colorimetric nanobiosensor targeting the Cry1Ac gene sequence.

Name	Sequence (5' → 3')	Length (bp)
Target Oligo	TTT AAA CTG AAG GCG GGA AAC G	22
Complementary Probe	C GTT TCC CGC CTT CAG TTT AAA	22

2.4. Support Vector Machine (SVM) Model Development

A supervised learning model based on a SVM classifier was implemented to correlate the optical responses of the AuNP nanobiosensor with GMO content. UV–visible spectra ($400\text{--}700 \text{ nm}$, 10 nm intervals) obtained from three AuNP batches (Y5, Y6, Y8) were compiled into a dataset comprising more than 150 individual assays, representing five GMO classes (Non-GM, 25%, 50%, 75%, $\geq 98.4\%$ *w/w*). Two SVM models were developed to evaluate alternative feature representations of the colorimetric assay data. One model used the full optical density spectrum ($400\text{--}700 \text{ nm}$), while the other employed the $\text{OD}_{620}/\text{OD}_{520}$ ratio as a single feature reflecting gold nanoparticle aggregation and the

associated plasmonic red shift. Prior to model training, all features were standardized to zero mean and unit variance [32]. Model implementation was carried out in-house using the C programming language. Model parameters were selected using cross-validation within an 80/20 training–testing split, with stratification applied to preserve class balance. The final model was evaluated on a held-out test set and subsequently applied to independent external validation samples (RR soybean and GM cotton, $n = 4$) not included during training, providing a proof-of-concept assessment of model generalizability.

3. Results and Discussion

3.1. Characterization of AuNP

The properties of the synthesized AuNPs were characterized to assess their morphology, and size distribution. TEM micrographs (Figure 2a) revealed that the nanoparticles possessed uniform, spherical morphology with smooth surfaces and well-defined boundaries. Across all batches (S1, Y5, Y6, Y7, and Y8), the particles were evenly dispersed without visible aggregation, demonstrating the high colloidal stability of the citrate-reduced AuNPs. Particle-size distribution histograms (Figure 2b), generated from the analysis of more than 200 individual particles per batch, exhibited narrow and symmetric distributions with mean diameters ranging from 13 to 16 nm, depending on the synthesis conditions. Each histogram was normalized to the total particle count (0–100%) to enable direct cross-batch comparison. Over 90% of the particles fell within ± 1 nm of the mean diameter, confirming excellent monodispersity and high reproducibility of the synthesis process. The calculated mean diameters were 13.8 nm (S1), 13.4 nm (Y5), 15.2 nm (Y6), 15.8 nm (Y7), and 15.6 nm (Y8). All batches exhibited the characteristic wine-red color typical of well-dispersed, citrate-capped AuNPs, along with a consistent LSPR maximum near 520 nm. This combination of distinct optical features, uniform morphology, and narrow size distribution confirms the complete reduction of Au(III) ions and efficient stabilization by citrate anions.

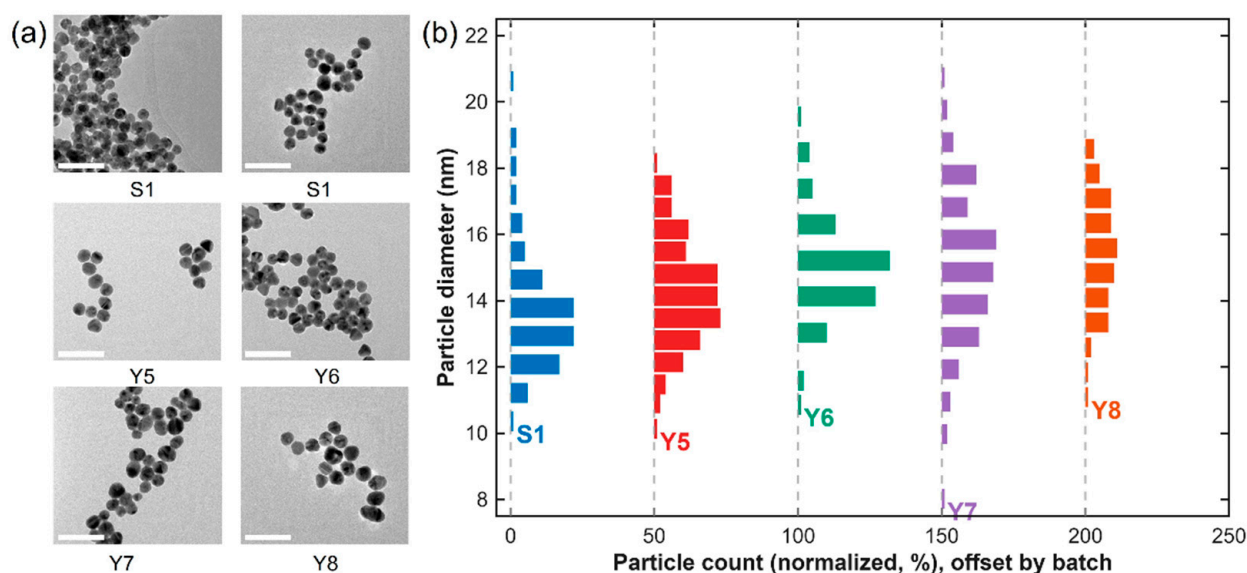


Figure 2. TEM micrographs and normalized particle-size distributions of AuNPs synthesized in batches S1, Y5, Y6, Y7, and Y8. (a) Representative TEM micrographs illustrating uniformly dispersed, quasi-spherical nanoparticles with minimal aggregation (scale bar = 50 nm). (b) Normalized particle-size distribution histograms centered between ≈ 13 and 16 nm, confirming narrow, symmetric size distributions and high batch-to-batch reproducibility. Each histogram is normalized to the total particle count (0–100%) to allow direct comparison among batches.

3.2. Effect of NaCl Concentration on AuNP Aggregation

To determine the optimal ionic conditions for controlled aggregation, citrate-stabilized AuNPs were exposed to progressively increasing NaCl concentrations, and their optical responses were monitored by UV–Vis spectroscopy. NaCl was selected as a simple and well-defined electrolyte to regulate AuNP aggregation by increasing ionic strength, thereby weakening electrostatic stabilization of the citrate layer and producing a reproducible plasmonic color change. Similarly, other monovalent electrolytes (e.g., KCl) are expected to promote aggregation in citrate-capped AuNP systems, since salt addition increases ionic strength and screens electrostatic repulsion between negatively charged nanoparticles, leading to plasmonic coupling accompanied by red-shift and broadening of the SPR band under comparable conditions [33]. Quantitative differences in aggregation kinetics or threshold concentration may arise due to ion-specific properties; however, the overall plasmonic coupling mechanism remains unchanged under comparable ionic strength conditions. Four NaCl concentrations (0.10 M, 0.15 M, 0.30 M, and 0.40 M) were initially tested (Figure 3a). Up to 0.10 M, both the solution color and SPR spectrum remained unchanged, indicating well-dispersed nanoparticles. At NaCl concentrations of 0.15 M and above, the solution color gradually shifted from red to purple–gray, accompanied by a red shift and broadening of the SPR band, confirming that increasing ionic strength screened electrostatic repulsion between citrate-capped AuNPs and promoted aggregation.

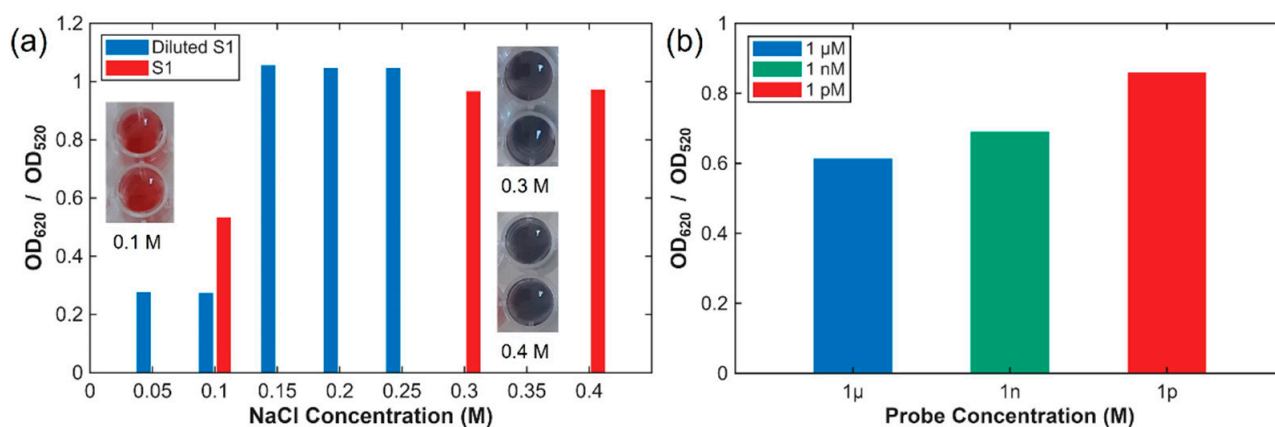


Figure 3. Effect of NaCl, particle, and probe concentration on AuNP aggregation. (a) OD_{620}/OD_{520} spectra of citrate-stabilized AuNPs exposed to 0.10–0.40 M NaCl, showing the onset of an SPR red shift above 0.15 M, indicative of aggregation. Secondary optimization using diluted AuNPs (≈ 1.5 nM) within the 0.05–0.25 M NaCl range confirmed the aggregation threshold near 0.15 M. (b) Probe-concentration-dependent variation of the OD_{620}/OD_{520} ratio across the pM, nM, and μ M range, demonstrating concentration-driven sensitivity.

The aggregation behavior of citrate-stabilized AuNPs was strongly influenced by both ionic strength and nanoparticle size. Smaller AuNPs required lower NaCl concentrations to induce aggregation, whereas larger particles exhibited aggregation at higher ionic strengths. This behavior is consistent with electrostatic screening effects, whereby increased ionic strength reduces effective surface charge repulsion and promotes size-dependent plasmonic coupling. Similar size- and ionic-strength-dependent aggregation behavior of citrate-capped AuNPs has been previously reported [24]. Based on these observations, NaCl concentrations in the range of 0.10–0.15 M were selected for subsequent assays, depending on nanoparticle batch characteristics.

A secondary optimization experiment was conducted using NaCl concentrations ranging from 0.05 to 0.25 M with a diluted S1 AuNP batch (1.5 nM) to evaluate the effect of nanoparticle density (Figure 3a). Aggregation again occurred near 0.15 M NaCl; however, the onset shifted slightly toward lower NaCl concentrations at reduced AuNP levels due

to decreased effective surface charge density and weaker electrostatic stabilization of the citrate layer. Based on these results, 0.15 M NaCl was selected as the standard condition for subsequent assays to ensure reproducible and sequence-specific colorimetric responses.

To further optimize the assay conditions, the effect of probe concentration on AuNP aggregation behavior was systematically investigated. As shown in Figure 3b, pronounced AuNP aggregation was observed at picomolar probe concentrations, whereas at micromolar concentrations the oligonucleotides strongly protected the nanoparticles against salt-induced aggregation, as evidenced by minimal absorbance changes in the 600–700 nm region. Because picomolar probe levels led to excessive aggregation and micromolar levels resulted in over-stabilization of the AuNPs, a probe concentration of 1 pM was selected as the optimal condition. At this intermediate level, a balanced interaction between the probe and AuNPs was achieved, enabling controlled aggregation and a distinct colorimetric response suitable for reliable discrimination across different probe concentrations relative to the control.

3.3. Detection of Genomic DNA

AuNPs were employed for sequence-specific detection of genomic DNA (gDNA) via salt-induced aggregation and the resulting colorimetric response. Complementary oligonucleotide probes targeting the Cry1Ac gene of GM soybean were hybridized with extracted gDNA representing five GMO classes (Non-GM, 25%, 50%, 75%, and $\geq 98.4\%$ *w/w*). The OD₆₂₀/D₅₂₀ ratio increased proportionally with both reaction time and GMO content, reflecting progressive aggregation driven by DNA hybridization. These optical changes directly correspond to molecular interactions between DNA strands and citrate-capped AuNP surfaces: single-stranded DNA adsorbs onto the nanoparticle surface and stabilizes the colloid against salt-induced coagulation, whereas double-stranded DNA does not, leading to aggregation. Consequently, increasing target DNA concentration enhances hybridization, reduces colloidal stability, and promotes AuNP clustering.

The performance of two different AuNP batches (Y6 and Y8) was evaluated at reaction times of 1, 5, and 10 min to assess their response and discrimination capability. Figure 4 summarizes the time-dependent colorimetric responses of two AuNP batches (Y6 and Y8) across different GMO levels. The performance of the batches was evaluated at reaction times of 1, 5, and 10 min to assess both kinetic behavior and discrimination capability. Panels (a) and (b) show the OD₆₂₀/D₅₂₀ ratios recorded at 1, 5, and 10 min for Y6 and Y8, respectively. For both batches, the absorbance ratio increased monotonically with increasing GMO content, indicating a concentration-dependent colorimetric response. Overall, Y6 and Y8 exhibited comparable trends and signal magnitudes across most GMO levels and reaction times. However, at the highest GMO content ($\geq 98.4\%$ *w/w*), Y6 displayed a slightly faster and stronger response, as evidenced by higher OD₆₂₀/D₅₂₀ values at early time points (Figure 4a), whereas Y8 reached similar levels more gradually (Figure 4b). The end-point comparison at 10 min (Figure 4c) confirms that both batches provide similar discrimination capability across GMO levels, with only marginal differences in signal magnitude. Overall, these results demonstrate that the assay enables rapid and semi-quantitative discrimination of GMO content within 10 min, while showing minimal batch-to-batch variation.

The specificity of the assay was evaluated using GM soybean as the Cry1Ac-positive target, while non-GM soybean and RR soybean were used as Cry1Ac-negative controls. In addition, GM cotton, which also contains the Cry1Ac gene, was intentionally included as a second positive target to assess gene-level specificity. As shown in Figure 5, Cry1Ac-negative samples (RR soybean and non-GM soybean) retained a red coloration, whereas Cry1Ac-positive samples (GM soybean and GM cotton) exhibited a significant shift toward a darker red-to-purple hue. Although the visual differences in the inset images

are subtle, the corresponding OD_{620}/OD_{520} ratios provide a clear quantitative distinction between target and non-target samples. Notably, GM cotton displayed a response comparable to that of GM soybean, confirming that the assay selectively detects the Cry1Ac gene rather than distinguishing between different Cry1Ac-containing GM events. Although DNA is a polyanionic molecule, the observed optical response is dominated by probe–target hybridization, as evidenced by the clear separation between Cry1Ac-positive and Cry1Ac-negative genomic DNA samples under identical assay conditions. These results demonstrate that the assay effectively discriminates Cry1Ac-containing targets from non-target samples and confirms its high sequence specificity, while enabling direct visual identification.

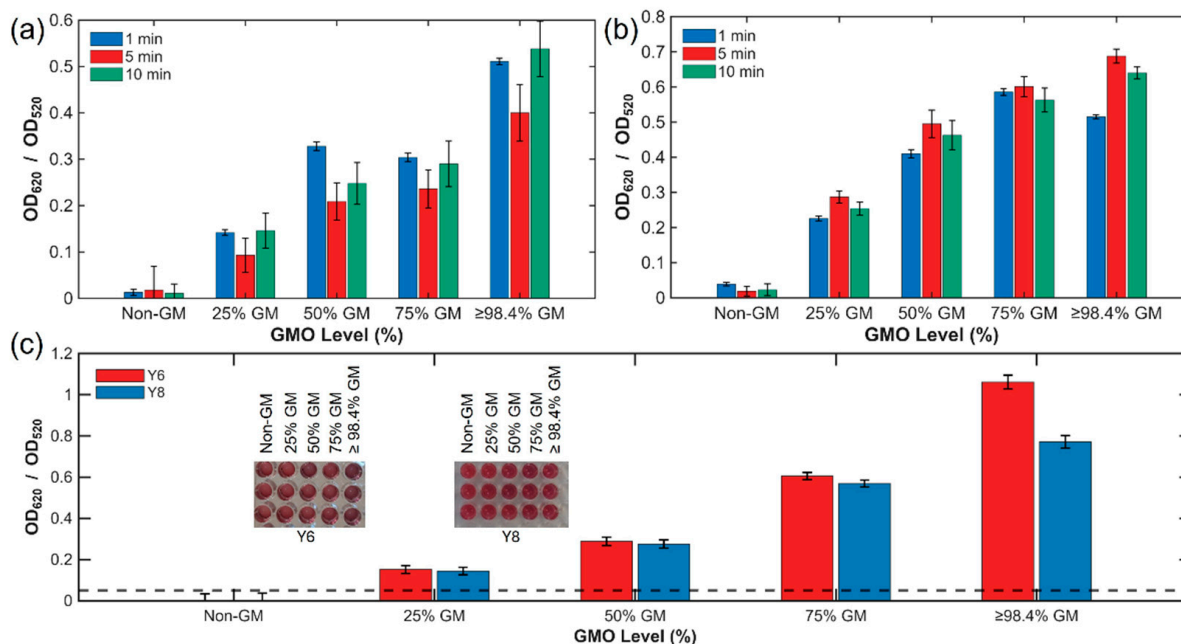


Figure 4. Detection of Cry1Ac genomic DNA from GM soybean using the AuNP-based colorimetric nanobiosensor. Five GMO levels, including non-GM ($<0.08\%$ w/w) and mixtures of extracted GM ($\geq 98.4\%$ w/w) and non-GM DNAs adjusted to 25%, 50%, 75%, and $\geq 98.4\%$ w/w , were hybridized with complementary probes and analyzed via salt-induced aggregation. (a) Batch Y6 (≈ 15.2 nm, 4.4 nm), and (b) Batch Y8 (≈ 15.6 nm, 4.77 nm) exhibit time-dependent increases in OD_{620}/OD_{520} ratios measured at 1, 5, and 10 min. (c) Endpoint spectra collected at 10 min demonstrate batch-to-batch reproducibility and nanoparticle-size-dependent sensitivity. The dashed line indicates the OD_{620}/OD_{520} ratio measured with the Cry1Ac-negative control (RR soybean DNA). Error bars represent $\pm SD$ ($n = 10$).

To evaluate analytical sensitivity, the limit of detection (LOD) was determined from the calibration curve as three times the standard deviation of the blank divided by the slope ($3\sigma/\text{slope}$), based on signal-to-noise ratios obtained from 10 min spectral data generated from three independent AuNP batches. This analysis yielded the lowest detectable DNA concentrations of 1.0 and 2.5 $\text{ng } \mu\text{L}^{-1}$ (depending on batch) for GM samples using batches Y6 and Y8, respectively. The slightly improved sensitivity observed for batch Y8 may be related to its particle size, which can influence plasmon coupling and enhance aggregation-induced optical shifts [34]. Overall, these results demonstrate excellent batch-to-batch reproducibility and confirm the high analytical sensitivity of the AuNP-based assay compared to other developed sensors.

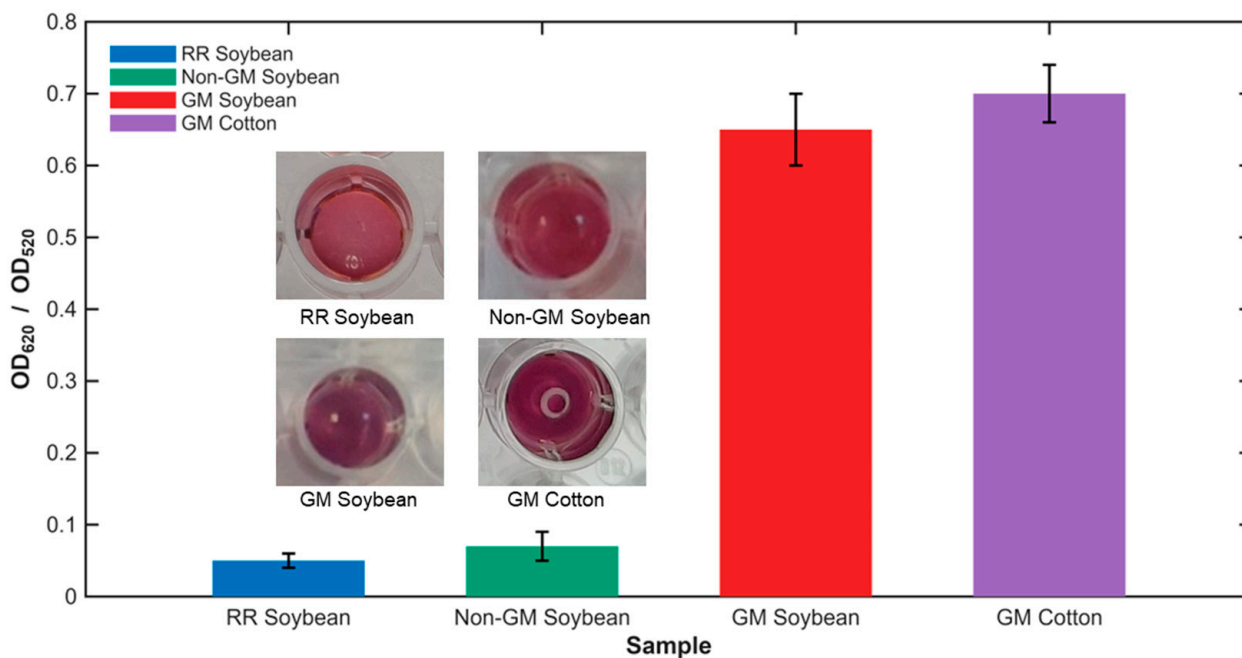


Figure 5. Representative visual and spectral responses are shown for Non-GM soybean (<0.08% *w/w*), RR soybean, GM soybean ($\geq 98.4\%$ *w/w*), and GM cotton ($\geq 99.6\%$ *w/w*). Target samples containing the Cry1Ac gene exhibit a pronounced red-to-purple color transition and elevated OD_{620}/OD_{520} ratios, whereas non-target samples remain red with minimal spectral changes. These results demonstrate high sequence specificity and negligible cross-reactivity of the assay.

3.4. Classification of GMO Levels Using SVM

The SVM analysis was performed using GMO concentration levels and corresponding UV–visible absorbance data obtained from AuNP-based colorimetric assays. Two feature representations were evaluated: (i) the normalized full absorbance spectrum recorded between 400 and 700 nm, and (ii) a reduced ratio-based feature defined as OD_{620}/OD_{520} , which captures the plasmonic red shift associated with nanoparticle aggregation. The SVM model was employed to classify samples into predefined GMO content categories and to support semi-quantitative discrimination, rather than to perform absolute quantitative determination as defined by regulatory reference methods.

Several kernel functions, including linear, polynomial, and radial basis function (RBF) kernels, were evaluated during model development. Among these, the RBF kernel consistently yielded the highest classification performance and was therefore employed in all reported analyses. When all AuNP batches were analyzed together using full-spectrum features, the SVM achieved a baseline classification accuracy of approximately 58%, which was limited by batch-to-batch spectral variability. To mitigate batch-dependent effects, SVM classification was subsequently performed on a per-batch basis using the RBF kernel.

SVM analysis was extended to AuNP batch Y5, in addition to batches Y6 and Y8, due to its smaller particle diameter. Batch Y5 demonstrated the highest classification performance, achieving accuracies of 95.5% using full-spectrum features and 93.3% using the ratio-based feature. In comparison, batches Y8 and Y6 achieved accuracies of 86.6%/55.5% and 63.4%/50%, respectively (Figure 6a). In this context, using the full spectrum preserves the overall spectral shape, including aggregation-induced peak broadening, red shifting of the ~ 520 nm LSPR band, and increased absorbance in the 600–700 nm region, whereas the OD_{620}/OD_{520} ratio reduces the information to two data points, which contributes to the improved classification performance observed with full-spectrum features. The heatmap in Figure 6b illustrates the overall classification performance across the three AuNP batches, highlighting clear differentiation between GMO classes and consistent intra-batch clas-

sification patterns. The superior performance of batch Y5 is attributed to its narrower size distribution and stronger LSPR confinement, which enhanced colorimetric contrast and spectral reproducibility [34]. The single misclassification observed during external validation corresponded to one GM cotton sample (GM Cotton 2) and was attributed to spectral variability rather than sequence variation, as the Cry1Ac gene targeted by the probe is conserved across Cry1Ac-containing GM events.

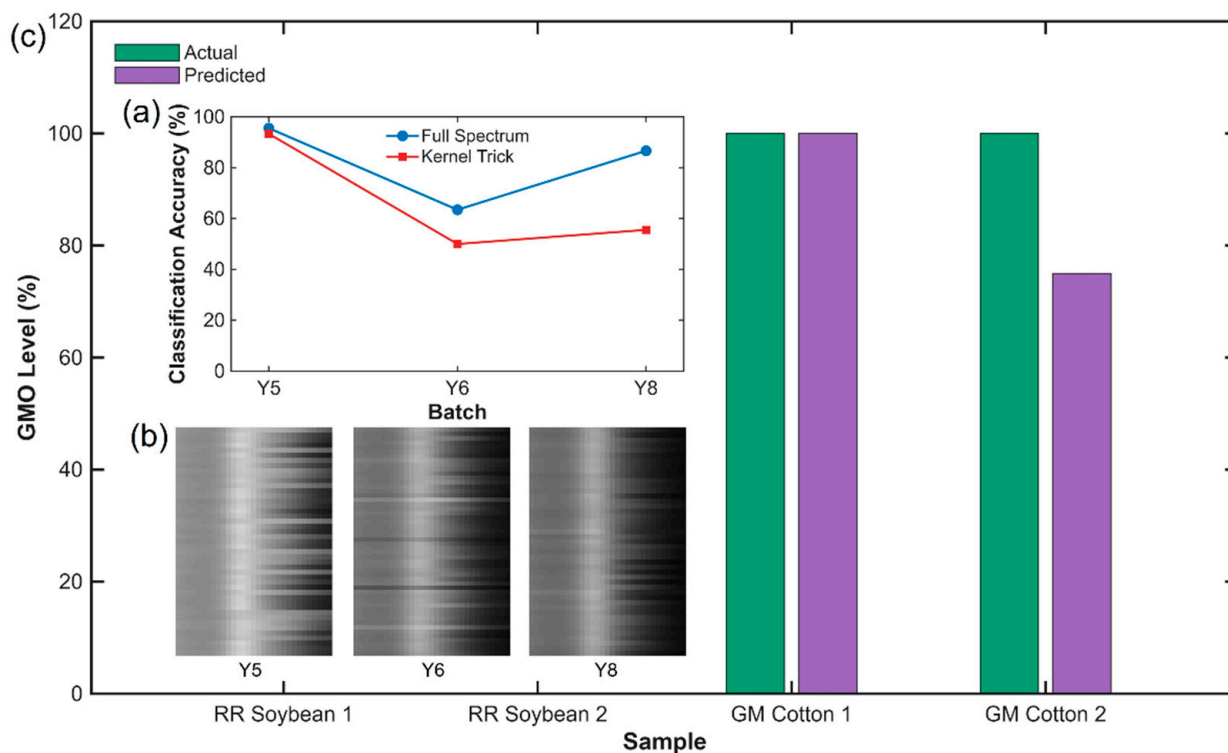


Figure 6. Machine learning-based classification of GMO levels using the SVM model. (a) Comparison of full-spectrum and ratio-kernel classification accuracies for three AuNP batches (Y5, Y6, and Y8). Batch Y5 achieved the highest accuracies (95.5% for full-spectrum and 93.3% for ratio-kernel data) due to its pronounced optical contrast and uniform aggregation behavior. (b) Heatmap representation of classification performance across the three AuNP batches. (c) External validation using four unseen genomic DNA samples, including two non-GM (RR soybean) and two GM (cotton), correctly classified three samples, corresponding to a 75% classification accuracy.

Overall, the integration of SVM-based machine learning with AuNP colorimetric sensing enabled semi-quantitative, amplification-free discrimination of GMO levels. The dependence of classification accuracy on nanoparticle size highlights the link between plasmonic field confinement and optical sensitivity. The modular design of the AuNP-based colorimetric assay also enables future multiplexing of event-specific probes for simultaneous detection of multiple GM markers, particularly when combined with machine-learning-assisted spectral classification. This synergy between nanophotonics and data-driven modeling establishes a foundation for intelligent, portable biosensors capable of rapid and automated GMO detection.

4. Conclusions

This study demonstrated a rapid, amplification-free colorimetric nanobiosensor for the detection of the Cry1Ac gene in the genetically modified soybean event MON87701, using gold nanoparticles (AuNPs) as optical transducers. Detection was based on direct hybridization between genomic DNA and complementary oligonucleotide probes, where salt-induced aggregation of citrate-stabilized AuNPs generated a visible red-to-

purple color transition proportional to the level of genetic modification. Under optimized ionic conditions (e.g., 0.15 M NaCl), the assay achieved a minimum detection limit of $\approx 2.5 \text{ ng } \mu\text{L}^{-1}$ (depending on batch), with relative standard deviations below 10%, confirming high analytical sensitivity and good reproducibility. Sequence specificity was verified using Cry1Ac-positive and Cry1Ac-negative genomic DNA. Only Cry1Ac-containing samples produced pronounced spectral shifts and color transitions, confirming selective probe–target hybridization. The influence of particle size on the optical response underscores the importance of nanoparticle size for optimal assay performance. Integration of the optical dataset with a SVM model enabled automated classification of five GMO levels (0%, 25%, 50%, 75%, 100%) with classification accuracies exceeding 90%. Overall, the developed AuNP-based nanobiosensor provides a fast, label-free, and cost-effective platform for qualitative and semi-quantitative GMO detection. Rather than replacing established PCR-based reference methods, the proposed system is positioned as a complementary, field-deployable pre-screening tool for food monitoring, traceability, and analytical decision support. The combined integration of nanoplasmonic sensing and machine-learning-assisted data interpretation supports the development of intelligent and portable biosensing systems applicable to agricultural biotechnology and broader nucleic-acid-based detection challenges.

Supplementary Materials: The following supporting information can be downloaded at: <https://www.mdpi.com/article/10.3390/bios16020128/s1>. Dataset for Figures and Tables (Excel file), containing the numerical data used to generate all figures and tables in the manuscript.

Author Contributions: Conceptualization, B.D. and R.Y.; methodology, Y.A. and R.Y.; software, Y.A.; validation, Y.T.K. and R.Y.; formal analysis, Y.A. and R.Y.; investigation, Y.T.K.; resources, R.Y.; data curation, Y.T.K. and Y.A.; writing—original draft preparation, Y.A.; writing—review and editing, Y.A., B.D. and R.Y.; supervision, B.D. and R.Y.; project administration, R.Y.; funding acquisition, R.Y. All authors have read and agreed to the published version of the manuscript.

Funding: This research was funded by Hacettepe University, grant number FHD-2019-17720.

Institutional Review Board Statement: Not applicable.

Informed Consent Statement: Not applicable.

Data Availability Statement: The data supporting the findings of this study are provided as Supplementary Material (Excel file).

Acknowledgments: The authors sincerely thank İlke Yılmaz for her creative contribution to Figure 1 and Saroopa Samaradivakara for constructive discussions that supported the experimental work.

Conflicts of Interest: The authors declare no conflicts of interest.

Abbreviations

The following abbreviations are used in this manuscript:

AuNP	Gold nanoparticle
CRM	Certified reference material
DNA	Deoxyribonucleic acid
dsDNA	Double-stranded DNA
EFSA	European Food Safety Authority
ELISA	Enzyme-linked immunosorbent assay
gDNA	Genomic DNA

GM	Genetically modified
GMO	Genetically modified organism
LOD	Limit of detection
LSPR	Localized surface plasmon resonance
NaCl	Sodium chloride
OD	Optical density
PBS	Phosphate-buffered saline
PCR	Polymerase chain reaction
PMEM	Post-market environmental monitoring
RBF	Radial basis function
SVM	Support vector machine
TEM	Transmission electron microscopy
UV-Vis	Ultraviolet-visible

References

- Naveen, A.K.; Sontakke, M. A Review on Regulatory Aspects, Challenges and Public Perception in Acceptance of Genetically Modified Foods. *Food Sci. Biotechnol.* **2024**, *33*, 791–804. [[CrossRef](#)] [[PubMed](#)]
- Sadikiel Mmbando, G.; Ngongolo, K. The Recent Genetic Modification Techniques for Improve Soil Conservation, Nutrient Uptake and Utilization. *GM Crops Food* **2024**, *15*, 233–247. [[CrossRef](#)] [[PubMed](#)]
- Warda, M.; Tekin, S.; Khafaga, N.; Sengul, E.; Çelebi, F.; Laçın, B.B. Comprehensive Insights Into Genetically Modified Foods: Technological Advances, Nutritional Benefits, Therapeutic Applications, and Health Implications. *Food Saf. Health* **2025**, *3*, 334–355. [[CrossRef](#)]
- Hamdan, M.F.; Tan, B.C. Genetic Modification Techniques in Plant Breeding: A Comparative Review of CRISPR/Cas and GM Technologies. *Hortic. Plant J.* **2025**, *11*, 1807–1829. [[CrossRef](#)]
- Baranski, R.; Klimek-Chodacka, M.; Lukasiewicz, A. Approved Genetically Modified (GM) Horticultural Plants: A 25-Year Perspective. *Folia Hort.* **2019**, *31*, 3–49. [[CrossRef](#)]
- Bekele-Alemu, A.; Dessalegn-Hora, O.; Safawo-Jarso, T.; Ligaba-Osena, A. Rethinking Progress: Harmonizing the Discourse on Genetically Modified Crops. *Front. Plant Sci.* **2025**, *16*, 1547928. [[CrossRef](#)]
- EFSA Panel on Genetically Modified Organisms (GMO). Guidance for Risk Assessment of Food and Feed from Genetically Modified Plants. *EFSA J.* **2011**, *9*, 2150. [[CrossRef](#)]
- European Union. European Parliament and Council Regulation (EC) No 1829/2003 on Genetically Modified Food and Feed. *Off. J. Eur. Union* **2003**, *L268*, 1–23.
- Shang, Y.; Xu, Y.; Huang, K.; Luo, Y.; Xu, W. Multiplex Pyrosequencing Quantitative Detection Combined with Universal Primer-Multiplex-PCR for Genetically Modified Organisms. *Food Chem.* **2020**, *320*, 126634. [[CrossRef](#)]
- Chaouachi, M.; El Malki, R.; Berard, A.; Romaniuk, M.; Laval, V.; Brunel, D.; Bertheau, Y. Development of a Real-Time PCR Method for the Differential Detection and Quantification of Four Solanaceae in GMO Analysis: Potato (*Solanum tuberosum*), Tomato (*Solanum lycopersicum*), Eggplant (*Solanum melongena*), and Pepper (*Capsicum annuum*). *J. Agric. Food Chem.* **2008**, *56*, 1818–1828. [[CrossRef](#)] [[PubMed](#)]
- Mano, J.; Hatano, S.; Nagatomi, Y.; Futo, S.; Takabatake, R.; Kitta, K. Highly Sensitive GMO Detection Using Real-Time PCR with a Large Amount of DNA Template: Single-Laboratory Validation. *J. AOAC Int.* **2018**, *101*, 507–514. [[CrossRef](#)] [[PubMed](#)]
- Niu, C.; Xu, Y.; Zhang, C.; Zhu, P.; Huang, K.; Luo, Y.; Xu, W. Ultrasensitive Single Fluorescence-Labeled Probe-Mediated Single Universal Primer–Multiplex–Droplet Digital Polymerase Chain Reaction for High-Throughput Genetically Modified Organism Screening. *Anal. Chem.* **2018**, *90*, 5586–5593. [[CrossRef](#)]
- Takabatake, R.; Kagiya, Y.; Minegishi, Y.; Yeasmin, S.; Futo, S.; Noguchi, A.; Kondo, K.; Mano, J.; Kitta, K. Development and Evaluation of Rapid Screening Detection Methods for Genetically Modified Crops Using Loop-Mediated Isothermal Amplification. *Food Chem.* **2018**, *252*, 390–396. [[CrossRef](#)]
- Singh, M.; Pal, D.; Aminedi, R.; Singh, A.K. Multiplex Real-Time Loop-Mediated Isothermal Amplification (LAMP) Based on the Annealing Curve Analysis: Toward an On-Site Multiplex Detection of Transgenic Sequences in Seeds and Food Products. *J. Agric. Food Chem.* **2024**, *72*, 17658–17665. [[CrossRef](#)]
- Liu, W.; Meng, L.; Liu, X.; Liu, C.; Jin, W. Establishment of an ELISA Method for Quantitative Detection of PAT/Pat in GM Crops. *Agriculture* **2022**, *12*, 1400. [[CrossRef](#)]
- Liu, H.; Wang, J.; Li, P.; Bai, L.; Jia, J.; Pan, A.; Long, X.; Cui, W.; Tang, X. Rapid Detection of P-35S and T-Nos in Genetically Modified Organisms by Recombinase Polymerase Amplification Combined with a Lateral Flow Strip. *Food Control* **2020**, *107*, 106775. [[CrossRef](#)]

17. Zeng, H.; Wang, J.; Jia, J.; Wu, G.; Yang, Q.; Liu, X.; Tang, X. Development of a Lateral Flow Test Strip for Simultaneous Detection of BT-Cry1Ab, BT-Cry1Ac and CP4 EPSPS Proteins in Genetically Modified Crops. *Food Chem.* **2021**, *335*, 127627. [[CrossRef](#)] [[PubMed](#)]
18. Chen, D.; Zhang, M.; Ma, M.; Hai, H.; Li, J.; Shan, Y. A Novel Electrochemical DNA Biosensor for Transgenic Soybean Detection Based on Triple Signal Amplification. *Anal. Chim. Acta* **2019**, *1078*, 24–31. [[CrossRef](#)] [[PubMed](#)]
19. Chou, C.-C.; Lin, Y.-T.; Kuznetsova, I.; Wang, G.-J. Genetically Modified Soybean Detection Using a Biosensor Electrode with a Self-Assembled Monolayer of Gold Nanoparticles. *Biosensors* **2022**, *12*, 207. [[CrossRef](#)]
20. Gil, B.; Keshavarz, M.; Wales, D.; Darzi, A.; Yeatman, E. Orthogonal Surface-Enhanced Raman Scattering/Field-Effect Transistor Detection of Breast and Colorectal Cancer-Derived Exosomes Using Graphene as a Tag-Free Diagnostic Template. *Adv. Nanobiomed. Res.* **2023**, *3*, 2300055. [[CrossRef](#)]
21. Ding, X.; Ge, D.; Yang, K.-L. Colorimetric Protease Assay by Using Gold Nanoparticles and Oligopeptides. *Sens. Actuators B Chem.* **2014**, *201*, 234–239. [[CrossRef](#)]
22. Nath, N.; Chilkoti, A. A Colorimetric Gold Nanoparticle Sensor To Interrogate Biomolecular Interactions in Real Time on a Surface. *Anal. Chem.* **2002**, *74*, 504–509. [[CrossRef](#)]
23. Baetsen-Young, A.M.; Vasher, M.; Matta, L.L.; Colgan, P.; Alocilja, E.C.; Day, B. Direct Colorimetric Detection of Unamplified Pathogen DNA by Dextrin-Capped Gold Nanoparticles. *Biosens. Bioelectron.* **2018**, *101*, 29–36. [[CrossRef](#)]
24. Mateos, H.; Mallardi, A.; Serrano-Pertierra, E.; Blanco-López, M.C.; Izzi, M.; Cioffi, N.; Palazzo, G. Unusual Gold Nanoparticle-Antibody Interactions. *JCIS Open* **2023**, *11*, 100089. [[CrossRef](#)]
25. Li, H.; Rothberg, L. Colorimetric Detection of DNA Sequences Based on Electrostatic Interactions with Unmodified Gold Nanoparticles. *Proc. Natl. Acad. Sci. USA* **2004**, *101*, 14036–14039. [[CrossRef](#)]
26. Ghazy, A.; Nyarku, R.; Faraj, R.; Bentum, K.; Woube, Y.; Williams, M.; Alocilja, E.; Abebe, W. Gold Nanoparticle-Based Plasmonic Detection of *Escherichia coli*, *Salmonella enterica*, *Campylobacter jejuni*, and *Listeria monocytogenes* from Bovine Fecal Samples. *Microorganisms* **2024**, *12*, 1069. [[CrossRef](#)]
27. Noble, W.S. What Is a Support Vector Machine? *Nat. Biotechnol.* **2006**, *24*, 1565–1567. [[CrossRef](#)] [[PubMed](#)]
28. Turkevich, J.; Stevenson, P.C.; Hillier, J. A Study of the Nucleation and Growth Processes in the Synthesis of Colloidal Gold. *Discuss. Faraday Soc.* **1951**, *11*, 55. [[CrossRef](#)]
29. Frens, G. Particle Size and Sol Stability in Metal Colloids. *Kolloid-Z. Z. Polym.* **1972**, *250*, 736–741. [[CrossRef](#)]
30. Schneider, C.A.; Rasband, W.S.; Eliceiri, K.W. NIH Image to ImageJ: 25 Years of Image Analysis. *Nat. Methods* **2012**, *9*, 671–675. [[CrossRef](#)] [[PubMed](#)]
31. Lucena-Aguilar, G.; Sánchez-López, A.M.; Barberán-Aceituno, C.; Carrillo-Ávila, J.A.; López-Guerrero, J.A.; Aguilar-Quesada, R. DNA Source Selection for Downstream Applications Based on DNA Quality Indicators Analysis. *Biopreserv. Biobank.* **2016**, *14*, 264–270. [[CrossRef](#)] [[PubMed](#)]
32. Kuhn, M.; Johnson, K. *Applied Predictive Modeling*; Springer: New York, NY, USA, 2013.
33. Wang, G.; Sun, W. Optical Limiting of Gold Nanoparticle Aggregates Induced by Electrolytes. *J. Phys. Chem. B* **2006**, *110*, 20901–20905. [[CrossRef](#)] [[PubMed](#)]
34. Link, S.; El-Sayed, M.A. Size and Temperature Dependence of the Plasmon Absorption of Colloidal Gold Nanoparticles. *J. Phys. Chem. B* **1999**, *103*, 4212–4217. [[CrossRef](#)]

Disclaimer/Publisher’s Note: The statements, opinions and data contained in all publications are solely those of the individual author(s) and contributor(s) and not of MDPI and/or the editor(s). MDPI and/or the editor(s) disclaim responsibility for any injury to people or property resulting from any ideas, methods, instructions or products referred to in the content.